Revised Version Submitted to Biological Cybernetics

RESPONSE LINEARITY DETERMINED BY RECRUITMENT STRATEGY IN DETAILED MODEL OF NICTITATING MEMBRANE CONTROL

Eirini Mavritsaki[1,3]

Nathan Lepora[1]

John Porrill[1]

Christopher H. Yeo[2]

Paul Dean[1]

[1]*Department of Psychology, Sheffield University, Sheffield, S10 2TP, U.K.*

[2]*Department of Anatomy and Developmental Biology, University College London, Gower Street, London WC1E 6BT, U.K.*

[3]*School of Psychology, University of Birmingham, Edgbaston, Birmingham B15 2TT, U.K.*

Running Head: Model of Nictitating Membrane Control

Correspondence to: Paul Dean, Department of Psychology, University of Sheffield, Western Bank, Sheffield S10 2TP, U.K.

E-mail: p.dean@sheffield.ac.uk

Phone: +44 114 222 6521

Fax +44 114 276 6515

Statement: EM and NL contributed equally to this work

Abstract

Many models of eyeblink conditioning assume that there is a simple linear relationship between the firing patterns of neurons in the interpositus nucleus and the time course of the conditioned response. However, the complexities of muscle behaviour and plant dynamics call this assumption into question. We investigated the issue by implementing the most detailed model available of the rabbit nictitating membrane response (Bartha and Thompson 1992a, 1992b), in which each motor unit of the retractor bulbi muscle is represented by a Hill-type model, driven by a non-linear activation mechanism designed to reproduce the isometric force measurements of Lennerstrand (1974). Globe retraction and NM extension are modelled as linked second order systems. We derived versions of the model that used a consistent set of SI units, were based on a physically realisable version of calcium kinetics, and used simulated muscle cross-bridges to produce force. All versions showed similar nonlinear responses to two basic control strategies. (i) Rate-coding with no recruitment gave a sigmoidal relation between control signal and amplitude of conditioned response, reflecting the measured relation between isometric muscle force and stimulation frequency. (ii) Recruitment of similar strength motor units with no rate coding gave a sublinear relation between control signal and amplitude of conditioned response, reflecting the increase in muscle stiffness produced by recruitment. However, the system response could be linearised by either a suitable combination of rate-coding and recruitment, or by simple recruitment of motor units in order of (exponentially) increasing strength. These plausible control strategies, either alone or in combination, would in effect present the cerebellum with the simplified virtual plant that is assumed in many models of eyeblink conditioning. Future work is therefore needed to determine the extent to which motor neuron firing is in fact linearly related to the nictitating membrane response.

1 Introduction

Classical conditioning of the eyeblink response and, especially, the closely-coupled nictitating membrane response (NMR) that is found in rabbits and a few other species, is an extensively studied model learning system. The neural mechanisms that underlie this learning have attracted considerable experimental interest, particularly since the discovery of cerebellar involvement (Hesslow and Yeo 2002, Llinás and Welsh 1993, Mauk et al. 2000, Thompson 1983). A key issue is how the cerebellum produces precisely timed conditioned responses (CRs), which ensure the eyelids are in place when the unconditioned stimulus arrives. It is therefore important to understand the relationship of cerebellar output, in this case the discharge of neurons in the interpositus nucleus, to movements of the eyelids and nictitating membrane.

There are currently two main views of this relationship. One is implicit in models of eyeblink conditioning that assume the time course of the CR to be a simple linear reflection of interpositus nucleus neuronal activity (Balkenius and Morén 1999, Fiala et al. 1996, Garenne and Chauvet 2004, Gluck et al. 2001, Hofstötter et al. 2002, Medina and Mauk 2000, Moore and Choi 1997). This assumption implies that the cerebellar signal can effectively ignore the complexities of both brainstem circuitry and the mechanics of the plant that it controls.

The second view has been stated explicitly: "... it is somewhat unlikely that the actual discharge rate of interpositus neurons could be correlated with the profile of CRs determined from nictitating membrane displacement, as this is a passive, highly damped movement" (Delgado-García and Gruart 2005, p.375). The reference here is to the complex mechanics of the NMR, which is produced by retraction of the eyeball displacing Harder's gland and thus forcing the nictitating membrane (NM) across the cornea (Eglitis 1964). In fact control problems are posed not only by the NMR mechanics themselves, but also by substantial non-linearities in the response of the retractor bulbi muscle that acts on the globe. Lennerstrand (1974) recorded isometric force from both whole muscle and individual motor units, and in each case found a sigmoid response to input frequency with only a narrow linear range. It is thus far from obvious how the combined properties of retractor bulbi muscle and NMR mechanics could be controlled in the simple linear manner postulated by models of eyeblink conditioning.

Recording studies have shown that there are neurons in and around the interpositus nucleus in rabbit and rat that start to fire shortly before CR onset (either eyelid or NM), and have activity profiles that resemble the time course of the CR (Aksenov et al. 2004, Berthier et al. 1991, Berthier and Moore 1990, Choi and Moore 2003, Freeman and Nicholson 2000, McCormick and Thompson 1984). For some neurons this relationship is linear (Berthier et al. 1991), and indeed for some the activity is not '"a mere increase or decrease in firing rate but what seems to be a complete copy of the behavioral response with varying degree of lead times" (Choi and Moore 2003, p.1217). However, other neurons in these studies do not show such simple relationships, and in cat many blink-related neurons in the posterior interpositus nucleus only start to fire after CR onset (Delgado-García and Gruart 2005). It is possible that some of these discrepancies reflect differences in the properties of the relevant C2 and C3 zones of the cerebellum (Choi and Moore 2003, Hesslow and Yeo 2002), but until this question can

be resolved the direct experimental evidence remains ambiguous with respect to the two views stated above.

An alternative way of throwing light on this issue is to use a different type of model, that specifically simulates the processes linking neuronal behaviour in the interpositus nucleus to NMR production. Although to our knowledge such a model is not available in its entirety, a major portion of it has been developed by Bartha and Thompson (1992a, 1992b) who have related the NMR of rabbits to the firing patterns of motoneurons (MNs) in the accessory abducens nucleus. Since their model successfully reproduces the non-linearities of retractor bulbi behaviour recorded by Lennerstrand (1974), it is well suited to the identification of control signals that could overcome them. Moreover it has the great advantage of being a distributed model in which MNs are represented as a population, so that the effects of a recruitment strategy can be investigated.

We describe here an implementation of Bartha and Thompson's model that addresses a number of problems in the original version, and show that its responses can be linearised when the simulated motor units are recruited appropriately. Parts of this work have been presented previously in abstract form (Lepora et al. 2005, Mavritsaki et al. 2001)

2 Structure of Model

Bartha and Thompson's (1992a, 1992b) model of NMR production is organised into three parts (Fig 1). The first part describes how isometric force is produced by a spike input

Figure 1 about here

train, based on the underlying microscopic properties of the muscle. The second part finds the associated dynamical force, which depends on the lumped muscle properties of length and velocity. Finally, the third part represents the motion of the eyeball and NM as a coupled, second-order linear system. In this section we describe the equations used in each part of the model, and give the values of the equation parameters (Table 1). Some of these values differ from those in the corresponding table

Table 1 about here

for the original model (Bartha and Thompson 1992a, Table 1), for reasons explained below.

2.1 Isometric Force Model for an Individual Motor Unit

The first part of the model converts an arbitrary train of spikes from an accessory abducens motoneuron into the time-varying isometric force produced by its motor unit in the retractor bulbi muscle. MN firing is represented as a discrete time series of action potentials arriving at the neuromuscular junction

$s = (s_0, s_1, s_2, \cdots)$ at $t = (0, \Delta t, 2\Delta t, \cdots)$.

Each individual value $s_n = 0 \text{ or } 1$ of this series denotes either the presence or absence of a spike input at time $n\Delta t$.

Each action potential then affects the muscle by releasing an activating substance, some of which becomes bound by the muscle and thereby produces muscle force. Activator kinetics are represented by two equations derived from Stein and Wong (1974)

$$\frac{dA}{dt} = -k_1\left(1-\frac{B}{B_m}\right)A - k_2\left(\frac{A}{A+A_{k_2}}\right)A + \left(1-\frac{A}{A_m}\right)R(t), \quad (1)$$

$$\frac{dB}{dt} = k_1\left(1-\frac{B}{B_m}\right)A - k_3\left(\frac{A_{k_3}}{A_{k_3}+A}\right)B, \quad (2)$$

where *A* is the concentration of activator in the sarcoplasm that is available for binding, *B* the concentration of activator bound to the myofilaments, k_1, k_2 and k_3 are rate constants, and A_{k_2}, A_{k_3}, A_m and B_m are constants introducing various saturating nonlinearities into the system (Fig 2). The term

Figure 2 about here

R(t) describes the release of activator by action potentials delivered at $t_i = t_1, t_2, \ldots$,

$$R(t) = \sum_i A_b f(t_{\text{ipi}}[i])\delta(t - t_i), \tag{3}$$

$$f(t_{\text{ipi}}) = 1 + f_{\max}(t_{\text{ipi}}[i]/t_{\max})^2 \exp[2(1 - t_{\text{ipi}}[i]/t_{\max})], \qquad t_{\text{ipi}}[i] = t_i - t_{i-1}, \tag{4}$$

where A_b is the baseline level of activator release (i.e. with no facilitation), $t_{\text{ipi}}[i]$ is the time interval between two neighbouring spike stimuli, and f_{max} and t_{max} parameterise the non-linear 'facilitation' factor $f(t_{ipi})$, which is a function of the inter-pulse interval t_{ipi}. The isometric force f exerted by the motor unit is proportional to the concentration of bound activator

$$f = cB, \tag{5}$$

where c is an empirically determined constant.

2.2 Dynamical Force Model for Whole Muscle

In the second part of the model, isometric force is converted into the actual muscle force F_m by taking account of instantaneous muscle length and velocity, using a Hill type model. The actual force F exerted by the muscle at globe position x_{eye} and velocity v_{eye} is given by

$$F = L(x_{\text{eye}})F_v(v_{\text{eye}})\sum_i f_i + P(x_{\text{eye}}). \tag{6}$$

where f_i is the isometric force exerted by the i th motor unit, L is the active length-tension relation given in terms of x_{eye}, F_v the force-velocity relation given in terms of v_{eye}, and P the passive length-tension relation. This equation reflects the assumption that all muscle fibres have the same length and move with the same velocity, so that the length and velocity terms are common to every motor unit and can be simply multiplied by the summed isometric force. Active tension is a linear function of length

$$L(x_{\text{eye}}) = L_1 x_{\text{eye}} - L_2, \tag{7}$$

where L_1 and L_2 are constants. Force is related to velocity by a standard Hill equation

$$F_v(v_{\text{eye}}) = \left(1 - \frac{v_{\text{eye}}}{v_{\max}}\right) \Bigg/ \left(1 + \frac{F_{\max}}{a}\frac{v_{\text{eye}}}{v_{\max}}\right), \tag{8}$$

where $v_{\max}$ is the maximum velocity and F_{max}/a is a phenomenological constant. Finally, the passive tension is a spring term

$$P\left(x_{\text{eye}}\right) = k_p\left(x_{\text{eye}} - x_{\text{rest}}\right), \tag{9}$$

with elastic constant k_p and equilibrium position x_{rest}.

In the original model the total isometric motor unit force was taken to equal $\sum_{i=1}^{n} f_i = nf$, i.e. assuming that all n units produced the same force. This would occur if for example all units fired at equal frequencies and had equal strengths c.

2.3 Model of Orbital Mechanics

In the third part of the model, the muscle force retracts the globe and compresses Harder's gland to cause the nictitating membrane to move across the globe. This stage is represented by a model of the relevant mechanics (Fig 3), which includes the effects of globe movement on the length

Figure 3 about here

and velocity of the retractor bulbi muscle. The equations given here are slightly modified from the original, for reasons explained in the next section. The equations of motion are

$$M_{\text{eye}}\ddot{x}_{\text{eye}} = F_1 - F, \tag{10}$$

$$M_H\ddot{x}_{NM} = N\sin\theta - F_2 = F_1\tan\theta - F, \tag{11}$$

where M_{eye} and $\ddot{x}_{\text{eye}}$ are the mass and acceleration of the globe, M_{H} the mass of Harder's gland, $\ddot{x}_{NM}$ is the acceleration of the nictitating membrane, θ is a dimensionless coupling constant related to the geometry of Harder's gland, and F, F_1 and F_2 are the forces shown in Fig 3. Directions of positivity for x_{eye} and x_{NM} are indicated on Fig 3. The values of F_1 and F_2 are given by

$$F_1 = -k_g\left(x_{\text{eye}} + \sin\theta\, x_{NM} - x_{k_g}\right) - \nu_g\left(\dot{x}_{\text{eye}} + \sin\theta\,\dot{x}_{NM}\right), \tag{12}$$

$$F_2 = k_H\left(x_{NM} - x_{k_H}\right) - \nu_H\dot{x}_{NM}, \tag{13}$$

where k_g and k_{H} are the elasticities of the orbital tissue and Harder's gland, x_{k_g} and x_{k_H} the corresponding resting lengths, ν_g and ν_H their viscosities, and $\dot{x}_{\text{eye}}$ and $\dot{x}_{NM}$ the velocities of the globe and the nictitating membrane respectively.

3 Adjustments to Model

The three parts of the model described above were implemented in **MATLAB™** (code for generating all the figures is available from www.narg.com). A number of amendments to the original version were required. Minor corrections are described first.

3.1 Minor Corrections

3.1.1 Correction of Misprints

1. The original of equation (4) has an extra left bracket between the f_{max} and $t_{\text{ipi}}/t_{\text{max}}$ terms, which renders the full expression ambiguous (equation (4) in Bartha and Thompson (1992a); equation (9) in Bartha and Thompson (1992b)). Equation (4) is a re-arranged version of the original.

2. The original of equation (12) uses the term x_{k_h} instead of x_{k_g} (equation (11) of Bartha and Thompson (1992b)).

3. The claim that $\tan\theta = 4/12.5$ implies $\theta = 0.33$ radians (Bartha and Thompson 1992a, p.141) is incorrect. The correct value is 0.31 radians.

3.1.2 Units of Measurement

The parameter values shown in Table 1 are given in SI units (mass in kilograms, distance in metres, time in seconds), whereas those given in Table 1 of Bartha and Thompson (1992a) are expressed in a variety of units (mass in grams, distance in millimetres, time in either milliseconds or seconds). The conversion was straightforward except for the case of force, a derived unit with the dimensions of mass distance time^{-2}, which also appears in the parameters describing viscosity and elasticity of the globe and Harder's gland. Bartha and Thompson expressed the values of forces and force related quantities in units of grams (more correctly grams force). Our attempted replication of their results revealed that they had mistakenly used these quantities in the equations of motion as though grams force were equal to dynes (the CGI unit of force), thus omitting a conversion factor $g = 981$ cm/s^2 (the acceleration due to gravity). When the required correction factor is included their model shows unphysical behaviour. This problem and a proposed solution are outlined in Section 3.2.

3.1.3 Orbital Model Equations

1. The $\sin\theta\, x_{NM}$ terms in equation (12) have the opposite sign from those in equation (1) of Bartha and Thompson (1992a), which appear to have resulted from a sign error in calculating the spring tension F_1. Our equations of motion are now compatible with the observation that as x_{NM} increases, F_1 should decrease because it releases the spring compression.

2. Equation (11) now uses the correct $\tan\theta$ component of F_1, instead of $\sin\theta\cos\theta$ in equation (2) of Bartha and Thompson (1992a), . The $\tan\theta$ term is derived from considering the normal reaction $N = F_1/\cos\theta$ exerted by the eye on the Harder's gland. This has a minor effect since for the model value of $\theta = 0.31$ radians the difference between the two versions is marginal, but if θ were close to $\pi/2$ the normal reaction to balance F_1 becomes large when $\tan\theta$ is used, and small when $\sin\theta\cos\theta$ is used. The former reflects the actual geometrical arrangement more accurately.

3.2 Changes to Parameter Values

In addition to the minor corrections described above, three sets of changes to parameter values were needed for consistent and realistic performance.

3.2.1 Isometric Force

Some of the parameter values used to reproduce Lennerstrand's isometric force data in Figs 1-5 of Bartha and Thompson (1992b) were not identical to those shown in Table 1 of Bartha and Thompson (1992a). The variant values are shown in Table 2. The main effect of the alterations

Table 2 about here

was on the amplitude of the simulated twitch and tetanic responses: thus, the parameters used for Fig 3 of Bartha and Thompson (1992b) give amplitudes 20 -30% lower than those corresponding to the parameters in Table 1 of Bartha and Thompson (1992a). To obtain a single consistent set of parameters, the error between simulated results and experimental values was minimised over variation in muscle parameters (Table 2). Experimental data sets were taken from Lennerstrand's (1974) figures 2 (motor unit isometric twitch), 3 (effects of double pulse), and 5 (steady state tetanic tension as a function of frequency).

The mean square error between model and data sets were calculated, and summed to give the overall error measure to be minimised. This minimisation used the standard **MATLAB™** optimisation algorithm 'fminunc', which converged well when the weights for each error in the sum were all unity. The new parameter values are shown in Table 2 in the 'optimised' column, and the corresponding model performance illustrated in Fig 4. It can

Figure 4 about here

be seen that a consistent set of parameter values can be found to give a close match to the experimental data. These values typically differed from those in Table 1 of Bartha and Thompson (1992a) by less than 20%.

3.2.2 Orbital Mechanics

The original orbital tissue parameters k_g, x_{k_g}, k_H and x_{k_H} are not consistent with the two original constraints on orbital motion. These constraints were that: (i) the *in situ* resting positions of the globe and nictitating membrane are 15 mm and 0 mm; and (ii) the globe retraction and nictitating membrane extension have maximal values of 5 mm and 13 mm. While the resting positions at zero exerted force are accurate, simulations show the original parameter values give an actual maximal globe retraction and nictitating membrane extension of 4.5 mm and 14 mm respectively. Because there are four constraints (two each in (i) and (ii) above) for the four orbital tissue parameters, these parameters can be determined exactly. Table 1 gives the orbital tissue parameter values that are consistent with both original constraints. These new orbital tissue values differ only slightly from those used by Bartha and Thompson (when the units are appropriately chosen, as discussed below).

A more significant problem for the model of orbital mechanics follows from its incorrect use of grams for force (Section 3.1.2). In the original treatment, force-containing quantities like elasticity and viscosity were measured in grams/mm and grams/mm/ms. The use of grams for force is based on the convention that one gram-force is equal to 1 gram times the acceleration due to gravity. These factors for the gravitational acceleration were not included in the original model, making the original values for elasticity and viscosity inaccurate by a factor of g = 9.81 x 10^{-3} mm/ms^2. If correct values of the original parameters are used, the simulated response overshoots noticeably on its return to baseline, unlike actual responses and the claimed performance of the original model (Fig 5).

Figure 5 about here

A second-order mechanical system with inertia, viscosity and elasticity overshoots when it is underdamped, which occurs when its damping ratio ζ is less than one in

$$\zeta = \frac{\upsilon}{2\sqrt{mk}}, \tag{14}$$

where υ is viscosity, *k* is elasticity and *m* is mass. If the scaling by *g* is omitted for the original parameters a value of $\zeta = 4.5$ is obtained, whereas if *g* is included then $\zeta = 0.45$. These values correspond to the damped and underdamped responses in Fig 5a.

To rectify the overshoot problem, one or more of the model parameters for viscosity, elasticity or mass must be modified. Since the mass of the rabbit globe (3 grams) is based on direct measurements (Prince 1964), and the elasticities are fixed by the constraints on orbital motion (see above), this leaves viscosity as the only plausible candidate. The simplest method of restoring an overdamped response was to double the estimate for orbital tissue viscosity, which had only slight effects on the response amplitude and peak velocity, and modest increase in latency. The viscosity parameters giving the performance in Fig 5b are those in Table 1.

4 Physically Plausible Version of Model

Bartha and Thompson's model of muscle activation is derived from equations for calcium kinetics given in Stein and Wong (1974). However, two of the changes made by Bartha and Thompson raise concerns about the physical basis of their model. The following two subsections describe these concerns, and show how the model can be modified to allay them.

4.1 Activation Equations

The complex series of events intervening between the arrival of an action potential at the muscle and the generation of force has been modelled in two stages: (i) the calcium kinetics that link depolarisation to the formation of cross-bridges between muscle filaments, and (ii) the production of force by these cross-bridges.

4.1.1 Stein and Wong Equations

Stein and Wong (1974) modelled the binding and release of Ca^{2+} ions to and from the myofilaments by postulating a concentration *A(t)* of Ca^{2+} ions in the sarcolemma and a concentration *B(t)* of Ca^{2+} ions bound to the myofilaments, related in the simplest case by first-order kinetics:

$$\begin{aligned} \frac{dA}{dt} &= -\left(k_1 + k_2\right) A + k_3 B, \\ \frac{dB}{dt} &= k_1 A - k_3 B, \end{aligned} \tag{15}$$

where k_1 is the rate of binding Ca^{2+} from *A* to *B*, k_2 is the rate of losing *A* to the sarcoplasmic reticulum, and k_3 is the rate of disassociation from *B* to *A*. The k_1 and k_3 terms balance in the two equations, representing conservation of Ca^{2+} ions moving between *A* and *B*. The motivation for a simple system like (15) is that it yields a solution

$$B(t) = \frac{k_1 A_0}{\left(\alpha - \beta\right)}\left(e^{-\beta t} - e^{-\alpha t}\right), \tag{16}$$

where α and β are roots of the quadratic equation $s^2 + \left(k_1 + k_2 + k_3\right)s + k_2k_3 = 0$ and $A_0 = A(0)$ is the initial concentration of *A*. The solution (16) is identical to the γ-function used by Julian (1969) to model twitch activation in the Huxley (1957) cross-bridge model .

Two modifications to these first-order kinetics were made by Stein and Wong to include known non-linearities in muscle activation: a saturation of *B* and active transport of *A* to the sarcoplasmic reticulum. These changes resulted in the modified, non-linear rate equations

$$\begin{aligned}\frac{dA}{dt} &= -k_1\left(1-\frac{B}{B_m}\right)A - k_2\left(\frac{A_{k_2}}{A+A_{k_2}}\right)A + k_3B + R,\\ \frac{dB}{dt} &= k_1\left(1-\frac{B}{B_m}\right)A - k_3B,\end{aligned} \tag{17}$$

where B_m is the maximal concentration of *B* and A_{k_2} limits the rate of loss of *A* to the sarcoplasmic reticulum at relatively high concentrations of *A*. They also included a constant *R* parameter in the first equation to permit the possibility of continual release of Ca^{2+} ions into *A* from, say, repetitive neural activity.

4.1.2 Modifications by Bartha and Thompson

Bartha and Thompson modified the non-linear Stein-Wong model because it could not reproduce the experimental data of Lennerstrand. These modifications resulted in equations (1) and (2), reproduced here for convenience (see also Fig 2)

$$\begin{aligned}\frac{dA}{dt} &= -k_1\left(1-\frac{B}{B_m}\right)A - k_2\left(\frac{A}{A+A_{k_2}}\right)A + \left(1-\frac{A}{A_m}\right)R,\\ \frac{dB}{dt} &= k_1\left(1-\frac{B}{B_m}\right)A - k_3\left(\frac{A_{k_3}}{A+A_{k_3}}\right)B,\end{aligned}$$

where A_m is a new saturation concentration for *A*, and A_{k_3} limits the rate of loss of *B* to *A* at relatively high concentrations of *A*. The individual changes are as follows.

(i) The active transport rate term $k_2\,A_{k_2}\big/\left(A+A_{k_2}\right)$ of Stein and Wong is changed to $k_2A\big/\left(A+A_{k_2}\right)$. Whereas the original term decreased the rate at high concentrations of *A* relative to k_2, the modified term decreases the rate at low concentrations of *A*.

(ii) The original reverse reaction term k_3B for *B* to *A* is omitted. This change effectively ignores the effect of increasing the concentration of *A* as Ca^{2+} ions move from *B* to *A*. The reason given for ignoring this term is because the concentration of *B* is claimed to be much less than *A*, by which the term can only have negligible effect.

(iii) A term $(1 - A/A_m)$ that represents saturation of *A* at concentrations approaching A_m is added.

(iv) The kinetic term $-k_3B$ of Stein and Wong has been changed to $-k_3 B\, A_{k_3} \Big/ \left(A + A_{k_3} \right)$. This change treats the disassociation of *B* to *A* as an active transport term that is rate limited at high concentrations of *A* relative to A_{k_3}. The active transport term used by Stein and Wong depended upon the concentration of the initial state (*B* in this case), not the final state *A*.

Another change, not further discussed here, is that Bartha and Thompson allows the release term *R* to vary with time. This important modification allows a δ-function term to be used to simulate the release of Ca^{2+} ions from an individual action potential. A facilitation term can then be introduced to model the known non-linearities in activator release from successive action potentials.

4.1.3 Alternative Model

Bartha and Thompson saw the above changes as primarily heuristic, designed to reproduce the nonlinear behaviour of the retractor bulbi muscle described by Lennerstrand (1974). Hence they referred not to calcium but to an 'activator' (e.g. Fig 2). However, such a procedure may raise concerns about the physical basis of the resultant model, particularly in this case the omission of the reverse reaction from *B* to *A*. The aim of this section is therefore to investigate whether it is possible to restore the physical basis of Stein and Wong's original model while keeping the good fits to Lennerstrand's data obtained by Bartha and Thompson.

The differences caused by reversing the above changes (i-iii) are illustrated in Fig 6, for the

Figure 6 about here

model behaviour already shown in Fig 4. The main effect is to slow the return to baseline of isometric twitch tension (Fig 6a) and tetanic tension (Fig 6d). The lengthening of the twitch response elevates mean tetanic tension at sub fusion frequencies (Fig 6c). These effects are primarily the result of change (iii), i.e. post-peak twitch duration is increased by restoring the reverse reaction from *B* to *A*: changes (i) and (ii) on their own have small effects, which are in fact in the opposite direction (not shown). However, it is possible to find a set of values for the parameters in equations (1), (2), (3), (4) and (5) that restores the desired performance (Fig 6, grey line). These values are given in the figure legend, and are from 25 to 330 percent of the values in Table 1. It is thus in principle possible to restore much of the simplicity of Stein and Wong's (1974) activation model while fitting the data of Lennerstrand (1974).

It should be noted that reversing change (iv) changes model output in a way that cannot be compensated for by optimisation: the optimised fit for tetanus does not fuse at high frequencies and drops off too fast when the stimulus terminates, while the maximal tetanic force does not display the full sigmoidal shape of the frequency range to 200 Hz). Hence change (iv) of Bartha and Thompson is an essential part of the model.

4.2 Cross-bridge Modelling of Force Production

A central assumption in Bartha and Thompson's model is that muscle force is simply proportional to the amount of muscle activator *B*. However, the Stein and Wong activation equations were derived for use with the Huxley-Julian cross-bridge model. In this model the activator

concentration drives cross-bridge formation and contraction within the muscle, which is considerably more complicated than a simple linear relation. One approach that tests if the linearity postulate is reasonable is to compare the results from Bartha and Thompson's model with a model using cross-bridge dynamics to drive the force activation. An added benefit of using a cross-bridge model is that the Hill term in equation (8) then occurs naturally as a consequence of the cross-bridge dynamics.

In Stein and Wong's original formulation the concentration of bound Ca^{2+} *B* produces muscle force by altering the rate of cross-bridge formation in the Huxley-Julian cross-bridge model (Huxley 1957, Julian 1969). The formation and disassociation of cross-bridges are described by the first-order rate equation

$$\frac{\partial n}{\partial t}+\frac{sv}{2h}\frac{\partial n}{\partial u}=(1-n)f-ng, \tag{18}$$

where *n(u,t)* is the number of cross-bridges with normalised bond length *u* = *x/h* at time *t*, v is the velocity of muscle shortening, *s* is the sarcomere length, and *f* and *g* are *u*-dependant rates of making and breaking bonds. Huxley chose these rates to have a convenient form

$$f(u)=\begin{cases} f_1 u, & 0<u<1, \\ 0, & u\le 0, u\ge 1, \end{cases} \qquad g(u)=\begin{cases} g_1 u, & u>0, \\ g_2, & u\le 0, \end{cases} \tag{19}$$

where f_1, g_1 and g_2 are positive constants. Then the muscle force is the elastic tension generated by these cross-bridge bonds,

$$F(v,t)=k_0\int_{u=-\infty}^{\infty} nu\,du, \tag{20}$$

where k_0 relates to the elasticity of the cross-bridge bonds. To include muscle activation within the Huxley model, Julian weighted the rate of bond formation by an activation factor $\gamma(t)$, so that

$$f(u)=\begin{cases} \gamma(t) f_1 u, & 0<u<1, \\ 0, & u\le 0, u\ge 1. \end{cases} \tag{21}$$

At full activation $\gamma(t)$ = 1 the model behaves identically to the original Huxley model. At partial activation, a varying activator determines the time-dependence of the muscle force.

4.2.1 Cross-bridge Model: Equations and Parameters

In the cross-bridge version of Bartha and Thompson's model, the dynamic force produced by the retractor bulbi muscle is given by:

$$F(x_{\text{eye}},v_{\text{eye}})=L(x_{\text{eye}})\sum_i F_i(v_{\text{eye}})+P(x_{\text{eye}}), \qquad F_i=k_0\int_{u=-\infty}^{\infty} n_i u\,du, \tag{22}$$

where $L(x_{\text{eye}})$ and $P(x_{\text{eye}})$ are the active and passive length-tension relations and F_i is the force exerted by the i^{th} motor unit (cf equation (6): the new F_i term substitutes for both the previous F_i term and the

F-v relation). The cross-bridge dynamics for the *i* th motor unit $n_i(u,t)$ are governed by equation (18) with Stein and Wong's activation function

$$\gamma(t) = \frac{B(t)}{B_m}, \tag{23}$$

where B_m is the saturation concentration of the bound activator. The dynamic muscle force then drives the model of orbital mechanics as before. The full process can be represented by a similar system to that shown in Fig 1, but with a different interpretation of the isometric and dynamic parts of the model. Cross-bridge parameter values are chosen to fit the Hill curve parameters used by Bartha and Thompson (details of this non-trivial procedure are summarized in Appendix A). These values are given in Table 3. The parameter values for the Ca^{2+} dynamics must then be fitted to an appropriate

Table 3 about here

model behaviour. It proved possible to find two sets of parameters that would reproduce the performance of the original model, one for the original model's activation kinetics, the second for the changed kinetics described in section 4.1. The model performance shown in Fig 7 is for the original

Figure 7 about here

activation kinetics and is compared with the original experimental data from Fig 4.

5 Model Response to Control Strategies

Having shown that the model can fit available data with a consistent set of parameters (Section 3), and that it can be realised in a physically plausible manner (Section 4), we can now investigate the linearity of its responses to various control strategies. The first strategy to be considered is that used by Bartha and Thompson, which involves no recruitment and all motor units firing with the same frequency.

5.1 Frequency Modulation

When the number of units is kept constant and frequency is varied, the CR amplitude-frequency plots are sigmoid (Fig 8) with only a narrow linear range (around 0-40 Hz). It can be shown that this

Figure 8 about here

nonlinear behaviour is not generated by that part of the model dealing with orbital mechanics, as follows. Consider the equation of motion for the nictitating membrane in the form

$$K_1 \equiv M_{\text{eye}}\ddot{x}_{\text{eye}} - F_1 = -F(x_{\text{eye}}, \dot{x}_{\text{eye}}, t), \tag{24}$$

$$K_2 \equiv M_H \ddot{x}_{NM} - F_1 \tan\theta + F_2 = 0. \tag{25}$$

Here we are using K_1 and K_2 to denote the force terms on the left-hand side of these equations. These terms are defined by

$$F(x_{\text{eye}}, \dot{x}_{\text{eye}}; x_{NM}, \dot{x}_{NM})_1 = -k_g \left(x_{eye} + \sin\theta\, x_{NM} - x_{k_g} \right) - \nu_g \left(\dot{x}_{eye} + \sin\theta\, \dot{x}_{NM} \right), \tag{26}$$

$$F_2(x_{NM}, \dot{x}_{NM}) = k_H \left(x_{NM} - x_{k_H} \right) - \nu_H \dot{x}_{NM}. \tag{27}$$

Each of these terms K_1 and K_2 are linear because

$$K_i(\alpha\tilde{x}_{\text{eye}}, \alpha\dot{x}_{\text{eye}}, \alpha\ddot{x}_{\text{eye}}; \alpha\tilde{x}_{NM}, \alpha\dot{x}_{NM}, \alpha\ddot{x}_{NM}) = \alpha K_i(\tilde{x}_{\text{eye}}, \dot{x}_{\text{eye}}, \ddot{x}_{\text{eye}}; \tilde{x}_{NM}, \dot{x}_{NM}, \ddot{x}_{NM}), \tag{28}$$

for coordinates that are properly normalised to

$$\tilde{x}_{\text{eye}} = x_{\text{eye}} + \sin\theta x_{k_H} - x_{k_g}, \qquad \tilde{x}_{NM} = x_{NM} - x_{k_H}. \tag{29}$$

Then the linearity of the system depends only on the forcing term $F(x_{\text{eye}}, \dot{x}_{\text{eye}}, t)$.

In fact the sigmoidal response to frequency modulation (Fig 8) is a reflection of Lennerstrand's data (Fig 4c) for isometric force. The nonlinear shape of the isometric-force curve is determined by nonlinearities in the equations for muscle activation (equations (1) and (2)), and in the equations describing the effects of multiple input pulses (equations (3) and (4)).

5.2 Simple Recruitment

The second strategy to be considered is simple recruitment. It is simple because (i) any given unit either does not fire, or fires at a fixed frequency that is the same for all recruited units, and (ii) the strengths of all motor units are identical. The response of the model to this strategy is

Figure 9 about here

illustrated in Fig 9a. The amplitude of the NMR is approximately linear up until ~5 mm, then begins to curve over nonlinearly.

The nonlinearity of the response curves in Fig 9 derives from the equation linking dynamic force *F* to the number of active units *n*, the length-tension relation $L(x_{eye})$, the force-velocity relation $F_v(\dot{x}_{\text{eye}})$, innervation $I(s(t))$, and the passive tension term $P(x_{eye})$ (cf equation (6))

$$F(x_{\text{eye}}, \dot{x}_{\text{eye}}, t; n) = n\, L(x_{\text{eye}}) F_v(\dot{x}_{\text{eye}}) I(s(t)) + P(x_{\text{eye}}). \tag{30}$$

Here $L(x_{\text{eye}})I(s)$ is the active isometric force for a single motor unit. All of the functions in the forcing term $F(x_{\text{eye}}, \dot{x}_{\text{eye}}, t; n)$ are sources for non-linearity in the system. For illustration, suppose it were the case that NMR amplitude did depend linearly on the number of motor units (i.e. the curves that in Fig 9a were straight lines). If x_{NM}/n is to be constant, the system must be invariant with a scaling of both the response and unit number. Since K_i is also linear with the response, this can be true only if

$$F(\alpha\tilde{x}_{\text{eye}}, \alpha\dot{x}_{\text{eye}}, t; \alpha n) = \alpha F(\tilde{x}_{\text{eye}}, \dot{x}_{\text{eye}}, t; n). \tag{31}$$

Referring to the form of the forcing term, this linearity relation holds while

$$L(\alpha\tilde{x}_{\text{eye}})F_v(\alpha\dot{x}_{\text{eye}}) = L(\tilde{x}_{\text{eye}})F_v(\dot{x}_{\text{eye}}), \qquad P(\alpha\tilde{x}_{\text{eye}}) = \alpha P(\tilde{x}_{\text{eye}}). \tag{32}$$

In the original Bartha and Thompson model, none of the functions $L(x_{\text{eye}})$, $F_v(\dot{x}_{\text{eye}})$ or $P(x_{\text{eye}})$ satisfy this condition (equations (7), (8) and (9)). The effects of the velocity and passive-tension terms on the non-linearity of the response are, however, slight (data not shown). The main cause of the non-linearity in NMR amplitude is the length term in the Hill muscle model (equation (7)), as illustrated in Fig 9b. Because the elasticity of the muscle increases with the number of units recruited, the slope of the straight lines relating muscle tension to length increase. Since all the lines start from the same origin (the resting length of the muscle), they intersect the straight line relating orbital tissue tension to globe displacement in the manner shown. These intersection points correspond to the equilibrium positions of the system, which determine the amplitudes of the NMR. Thus, equal recruitment increments result in decreasing increments of NMR amplitude.

To conclude, simple recruitment produces a non-linear response of the system to unit number. This non-linearity may be a general property of systems where motor units are recruited and the load is elastic.

5.3 Recruitment Combined with Frequency Modulation

We investigated two methods of achieving a linear relationship between the number of MN spikes as input to the system, and the amplitude of the NMR. In the first method, the frequency of recruited motor units was allowed to vary (unit strengths remained equal). In the second, frequency was fixed as in the 'simple recruitment' strategy above, but the strength of the recruited units was allowed to vary. In principle, arbitrary combinations of these two strategies could be considered. In this report, we examine only these two individual cases as a proof of principle.

The problem in combining frequency modulation with recruitment is to determine how much frequency modulation is required. One method of solving this problem is shown in Fig 10. Fig 10a

Figure 10 about here

plots NMR amplitude as a function of both the number of recruited units and the frequency with which they all fire. On this plot, the two control strategies considered so far would correspond to straight lines parallel with the x-axis (frequency modulation) or with the y-axis (simple recruitment). The correct combination of recruitment and frequency modulation corresponds to a curve for which the total spike frequency $\omega = fn$ (where f is frequency and n the number of active units) is linearly related to the maximum NMR amplitude $a(f, n)$. These curves have

$$\frac{da}{d\omega} = c, \qquad a(f,0) = a(0,n) = 0, \tag{33}$$

with c a constant. These curves are the contour lines of the function a/ω, which can be plotted with the standard **MATLAB™** routine 'contourc(*f,n,a/ω*)'. These correspond to curves where the amplitude a is linearly related to total spike frequency ω.

Examples of such curves are shown on Fig 10a (dotted curves) with the linear relationship between amplitude and total spike frequency verified in Fig 10b. A striking feature of the curves in Fig

10a is that they all reach a maximum in unit number *n* at a frequency *f* about 110 Hz. This frequency corresponds to when the response saturates in Fig 8. Below 110 Hz the required recruitment strategy slightly increases firing frequency as more units become active, as indicated by the slight rightwards tilt of the ascending limb of the recruitment curves in Fig 10a.

5.4 Units of Differing Strengths

In the force equation (30) for the original model, all motor units are of the same strength. The simple recruitment strategy of section 5.2 then gives CR amplitudes that scale sublinearly with input. This problem could in principle be overcome by recruiting units that increased appropriately in strength, as is illustrated in Fig 11. In this example, the force term from equation (30) is scaled by a

Figure 11 about here

factor *f(n)* that increases faster than a linear relation to the number of units *n* but is normalized such that *f(100)=100*. This scaling results in a force

$$F(x_{\text{eye}}, \dot{x}_{\text{eye}}, t; n) = f(n)\ L(x_{\text{eye}})F_v(\dot{x}_{\text{eye}})I(s(t)) + P(x_{\text{eye}}), \tag{34}$$

Which at maximal recruitment $n_{\max}$=100 remains identical to Bartha and Thompson's original expression.

The particular choice of *f(n)* used in Fig 11 is based on an assumed exponential distribution for the strength of individual motor units. Supposing the *i* th unit strength is proportional to exp*(b i/*$n_{\max}$*)*, the constant *b* implies the strongest units are exp*(b)* times more powerful than the weakest units. Table 1 of Lennerstrand (1974) shows this proportion of strengths is about four-fold. Then these unit strengths imply an overall scaling

$$f(n) = \sum_{i=1}^{n} c\exp(b\,i/n_{\max}) = n_{\max}\left[\frac{1-\exp\left(b\,n/n_{\max}\right)}{1-\exp(b)}\right], \tag{35}$$

where *b=ln(4)* and the proportionality constant *c* is determined by $f(n_{\max})=n_{\max}$ to give the expression above.

Evidently, this scaling produces a more linear response of the system than simple recruitment. One might instead use a more complicated relation than the simple exponential scaling above to obtain a more linear response—in principle, a different scaling is possible for each of the 100 units. However, for the present purposes, the above model is sufficient to illustrate the principle that appropriate scaling of motor unit strength can linearise the system response.

6 Discussion

The results of this study suggest that the nonlinearities inherent in NMR production could in principle be overcome by an appropriate strategy for recruiting motor units in the retractor bulbi muscle. Use of such a linearising strategy would serve to reconcile the two conflicting views of conditioned NMR production described in the Introduction: models of eyeblink conditioning typically assume that the firing rates of interpositus neurons are related in simple fashion to the time course of the CR, yet consideration of orbital mechanics and muscle non-linearities offers no basis for such an assumption. Suitable recruitment of motor units in effect presents the cerebellum with a simplified virtual plant.

We discuss the nature of the nonlinearities incorporated in the model of Bartha and Thompson that was used in the present study; the plausibility of the strategies proposed to overcome them; Improvements to the model of orbital mechanics; and finally implications of the modelling results for the role of the interpositus nucleus in producing conditioned responses.

6.1 NMR Nonlinearities

Two major nonlinearities in NMR production were identified in Bartha and Thompson's model, one in the relation of isometric force to rate coding (Figs 4c, 8c), the other in the length-tension relation as affected by recruitment (Fig 9).

6.1.1 Isometric Tension versus Frequency

The sigmoidal relation between isometric tension and frequency of stimulation has long been known (Cooper and Eccles 1930), and has been demonstrated for individual motor units of skeletal muscle (Kernell et al. 1983), of the retractor bulbi muscle (Lennerstrand 1974), and of the extraocular muscles that rotate rather than retract the eye (Goldberg 1990). The sigmoidal relation therefore appears to be a ubiquitous feature of striated muscle, with only the frequency range of the linear portion varying from motor unit to motor unit.

The origins of the sigmoidal relation lie in the cascade of nonlinear dynamic processes that intervene between stimulation and force production, which includes release of calcium from the sarcoplasmic reticulum by depolarisation, calcium kinetics inside the sarcoplasm, interaction of calcium with troponin and hence cross-bridge formation, and the effects of cross-bridge formation on intrinsic muscle viscoelasticity. These processes, which for calcium kinetics have probably been most studied in cardiac muscle (Bers 2002) , are sufficiently complex that no generally accepted detailed model relates them to overall muscle behaviour (e.g. Curtin et al. 1998, Neidhard-Doll et al. 2004, e.g. Shames et al. 1996, Zahalak and Motabarzadeh 1997). As a result, most models concerned with nonlinearity of isometric force production in skeletal muscle have used lumped equations whose parameters have a distant relation to underlying biophysics (e.g. Bobet and Stein 1998, Brown and Loeb 2000, Ding et al. 2002, Dorgan and O'Malley 1998, e.g. Hannaford 1990, Shadmehr and Arbib 1992, Watanabe et al. 1999). The main criterion for their utility is how well they fit the experimental data, as indicated in a recent evaluation of seven models for skeletal muscle (Bobet et al. 2005).

The present model based on the work of Bartha and Thompson uses the same general approach as the lumped-equation models of skeletal muscle, and its fits to the relevant experimental data (Fig 4) appear to be at least as good those for the seven models evaluated by Bobet et al. (2005). Moreover, as we have shown here, similar fits for the retractor bulbi model can be obtained with a more biophysically based set of equations (Figs 6, 7), suggesting that it may be possible to extend the model as further information about the detailed processes underlying muscle calcium kinetics becomes available. However, its present form seems adequate for purpose of reproducing known nonlinearities in isometric force production by the retractor bulbi muscle.

6.1.2 Recruitment Nonlinearity

Recruitment of motor units increases muscle stiffness, and thus alters the equilibrium length of the muscle when it is faced with an elastic load (Fig 9b). This feature is recognised and exploited by the equilibrium point hypothesis for the control of joint angle by agonist and antagonist muscles (Bizzi et al. 1982, Feldman 1981). However, its importance in the present context is that recruiting units of equal strength does not produce equal increments in equilibrium position of the nictitating membrane (Fig 9b), but instead gives a sublinear relationship between NMR amplitude and number of recruited units (Fig 9a). This relationship would follow from any model of muscle behaviour in which the elasticities of recruited motor units were identical.

6.2 Plausibility of Proposed Linearising Mechanisms

In the model we show that the NMR response to motoneuron input can be linearised either by appropriate combination of recruitment and rate coding, or by recruiting motor units in order of increasing strength. Both these strategies are widespread in the skeletal motor system, and it has been demonstrated that a combination of recruitment and rate coding can linearise the force response to functional electrical stimulation (Zhou et al. 1987). Recruitment and rate coding also occur in the eye-movement control system, and there is some indirect evidence for the size principle (Dean 1996, Dean et al. 1999). In general terms the suggested mechanisms for linearisation of the NMR are therefore perfectly plausible, and indeed recruitment has already been proposed as the main mechanism for controlling the amplitude of eyelid responses (Gruart et al. 1995).

However, there is little specific evidence for a linear response to MN firing in conditioned NMRs. Single unit studies have either been very preliminary (Berthier and Moore 1983, Disterhoft and Weiss 1985), or carried out in cat (Trigo et al. 1999) where it appears that, unlike in rabbit (Leal-Campanario et al. 2004), accessory abducens MNs do not fire during conditioned blinks. An early study of multi-unit MN firing in rabbit showed activity profiles that strongly resembled, and were highly correlated with, the time-course of the NMR (Cegavske et al. 1979, Fig 8). The authors concluded that "[w]hatever the abducens units do, so will the NM do" (p.605). However, the recordings were from the abducens rather than accessory abducens, only four examples of relevant data are shown, and no explicit demonstration of linearity was undertaken. Acquiring further data on the relation between MN firing and the NMR is thus an important step in furthering our understanding of how the cerebellum controls conditioned NMRs.

6.3 Improving the Orbital Mechanics Model

Whereas Bartha and Thompson were able to validate the part of their model dealing with isometric force production by direct comparison with Lennerstrand's (1974) stimulation data for the retractor bulbi muscle, equivalent data for the relevant orbital mechanics were not available. In the absence of relevant measurements they assumed that the mechanics could be represented by a linear viscoelastic system, with coefficients estimated as best as possible from available data. The elasticity of orbital tissue was calculated from the maximum force exerted by the retractor bulbi muscle divided by the maximal retraction of the eyeball, and the viscosity was estimated from the observation that the maximum force exerted by the retractor bulbi muscle, acting for 30 ms, produces a retraction velocity of 100 mm/s and a peak NM velocity of 250 $mm.s^{-1}$. The orbital mechanics model was validated by demonstrating the plausibility of (i) the NMRs produced by either short-duration high-frequency bursts of MN firing, or inputs patterned after (the scant) neurophysiological data, and (ii) the MN firing patterns required to produce actual CR profiles (assuming no recruitment). Bartha and Thompson argued in addition that, despite the uncertainties inherent in these estimation procedures, the model was robust and not "overly sensitive to parameters changes" (p.142).

We were unexpectedly able to confirm this robustness. It turned that the values for plant elasticities and viscosities actually used by Bartha and Thompson were in fact ~1/100th of the stated values, and that restoring the latter had relatively modest effects on the simulated NMR (Fig 5a) beyond the conversion from an overdamped to an underdamped response. Performance close to the original could be re-instated by subsequent doubling of viscosity (Fig 5b). However, it would clearly be an improvement to base the model on actual measurements, and it is perhaps surprising that these have apparently not been carried out in the years since the model was first published.

Although not to be regarded as a simple improvement to the present model, the construction of an equivalent model for the external eyelid response would also be highly desirable. There is indirect evidence for linearity in eyelid responses (Evinger et al. 1991, Gruart et al. 1995, Gruart et al. 2000, Trigo et al. 2003), and a start on a detailed model appears to have been made (Hung et al. 1977, Sanchez-Campusano et al. 2003).

6.4 Implications for Role of Interpositus Nucleus in Control of Conditioned Eyeblinks

The present results indicate that appropriate recruitment of MNs in the rabbit accessory abducens nucleus presents premotor areas with a simplified virtual plant, allowing them to code the desired movement of the nictitating membrane in a straightforward fashion. As described in the Introduction, such coding is assumed for the interpositus nucleus and conditioned eyeblink responses in many models of eyeblink conditioning, and is consistent with the firing patterns of some interpositus neurons. However, important issues remain to be resolved. One is that there are other neurons in and around the interpositus nucleus whose firing is not related to conditioned response dynamics in a simple way (Introduction). The functional role of these neurons remains to be clarified, perhaps particularly in relation to differences between species. Secondly, it is unclear how the required recruitment pattern of MNs might be organised. The interpositus nucleus does not project directly to the accessory abducens nucleus, but indirectly via the red nucleus (Hesslow and Yeo 2002). Very little

is known about the functions of this relay station: perhaps one of them is to coordinate the required recruitment of accessory abducens MNs.

6.5 Summary

1. Bartha and Thompson's detailed model of NMR production was implemented in MATLAB™, using a consistent set of SI units.
2. Its performance was reproduced by alternative versions of the model that incorporated more realistic calcium kinetics, and force production by cross-bridge formation.
3. Two main sources of nonlinearity were identified, namely the sigmoidal relation between NMR amplitude and input frequency for rate coding, and a sublinear relationship between NMR amplitude and number of units recruited for a simple recruitment strategy.
4. A linear relation between number of input action potentials and NMR amplitude could be achieved either by appropriate combination of rate coding and recruitment, or by suitable increase in motor unit strength with recruitment.
5. A linearising recruitment strategy could in principle underpin the assumption made in many models of the cerebellar control of conditioned NMRs, that there is a simple relation between response profiles and the firing patterns of units in the interpositus nucleus.

Appendix

Parameter Values for Cross-bridge Model

Huxley (1957) used values for the rate constants f_1, g_1 and g_2 that reproduced the behaviour of Hill's equations when $a/F_0=0.25$. The model considered here uses the slightly larger value $a/F_0=0.3$ from Table 1, which means Huxley's original values are not valid. Parameter estimation was achieved by comparing the cross-bridge model at full activation $\gamma=1$ to the Hill equations for particular values of a/F_0, F_0 and $v_{\max}$. The resulting parameter values are summarised in Table 3 below.

Table 3 about here

(i) The ratio s/h determines the time that the cross-bridge model takes to reach a steady state of constant force, since in equation (18) it scales the velocity of muscle shortening to the velocity of sarcomere shortening relative to characteristic bond length h. Simulations revealed a value $h/s=1/10000$ gives a characteristic time scale of a few milliseconds. In practice, a time scale less than the twitch time scale (10 ms) is needed to obtain a realistic twitch response.

(ii) Huxley identified the Hill parameter $b=(a/F_0)v_{\max}$ with the quantity $h/s(f_1+g_1)$ that naturally scaled the maximal velocity $v_{\max}$ in his exact solution to the cross-bridge model. Hence

$$f_1 + g_1 = \frac{s}{h}\frac{a}{F_0} v_{\max}. \tag{36}$$

The values from Table 1 lead to $f_1+g_1=1320$.

(iii) Huxley found the parameter ratio g_2/f_1+g_1 from his exact solution (11) for muscle force in the cross-bridge model. Using (36) above, (11) from Huxley and the condition $F(v_{\max})=0$ leads to the expression

$$\frac{g_2}{f_1+g_1} = \left[\left(\frac{a}{F_0} \right)^2 \frac{2}{1-e^{-a/F_0}} - 2\frac{a}{F_0} \right]^{-1/2}. \tag{37}$$

Substituting the value $a/F_0=0.3$ gives $g_2/f_1+g_1=3.25$.

(iv) The parameter ratio g_1/f_1+g_1 can only be fixed by comparing the energetics of muscle function in the cross-bridge model and Hill equations. The rate of energy liberation from muscle shortening in the cross-bridge model is

$$E = e_0 \int_{u=-\infty}^{\infty} (1-n) f(u) du, \tag{38}$$

where e is related to the energy released each time a cross-bridge forms. Huxley then related the maintenance heat rate E_0 (rate of energy liberation for isometric muscle function) to the value $E_0=ab=(a/F_0)^2F_0v_{\max}$ quoted in Hill's paper. The exact expression (9) from Huxley then leads to

$$e_0 = \frac{h}{s}\frac{a}{F_0}\frac{f_1+g_1}{g_1} k_0. \tag{39}$$

Thus the overall scale of energy liberation is inversely proportional to g_1/f_1+g_1. This scale can then be fixed by comparing the prediction from (38) with the rate of energy liberation in Hill's equations

$$E = \left(\frac{a}{F_0} \right)^2 F_0 v_{\max} + (a + F) v \tag{40}$$

for muscle force $F=F_0F_v$ at shortening velocity v. The value $g_1/f_1+g_1=0.21$ gives the fit in Fig 7.

(v) The k_0 parameter in (20) is proportional to active isometric force produced by the muscle. Huxley derived the exact expression for this force

$$F_0 = \frac{k_0}{2} \frac{f_1}{f_1 + g_1}. \tag{41}$$

In practice, simulations revealed that full activation does not occur even at very high stimulation frequencies, so the above equation overestimates the maximal tetanic force. For this reason a value $k_0=0.87$ was used in our simulations, which is slightly less than the value predicted by (41).

Acknowledgements

This research was supported by the UK Biotechnology and Biological Sciences Research Council (grant BBS/B/17026, and Research Committee studentship to E.M.).

References

Aksenov D, Serdyukova N, Irwin K, Bracha V (2004) GABA neurotransmission in the cerebellar interposed nuclei: Involvement in classically conditioned eyeblinks and neuronal activity. Journal of Neurophysiology 91:719-727

Balkenius C, Morén J (1999) Dynamics of a classical conditioning model. Autonomous Robots 7:41-56

Bartha GT, Thompson RF (1992a) Control of rabbit nictitating membrane movements: 1. A computer model of the retractor bulbi muscle and the associated orbital mechanics. Biological Cybernetics 68:135-143

Bartha GT, Thompson RF (1992b) Control of rabbit nictitating membrane movements: II.Analysis of the relation of motoneuron activity to behavior. Biological Cybernetics 68:145-154

Bers DM (2002) Cardiac excitation-contraction coupling. Nature 415:198-205

Berthier NE, Barto AG, Moore JW (1991) Linear systems analysis of the relationship between firing of deep cerebellar neurons and the classically conditioned nictitating membrane response in rabbits. Biological Cybernetics 65:99-106

Berthier NE, Moore JW (1983) The nictitating membrane response: An electrophysiological study of the abducens nerve and nucleus and the accessory abducens nucleus in rabbit. Brain Research 258:201-210

Berthier NE, Moore JW (1990) Activity of deep cerebellar nuclear cells during classical conditioning of nictitating membrane extension in rabbits. Experimental Brain Research 83:44-54

Bizzi E, Accornero N, Chapple W, Hogan N (1982) Arm trajectory formation in monkeys. Exp Brain Res 46:139-143

Bobet J, Gossen ER, Stein RB (2005) A comparison of models of force production during stimulated isometric ankle dorsiflexion in humans. IEEE Transactions On Neural Systems And Rehabilitation Engineering 13:444-451

Bobet J, Stein RB (1998) A simple model of force generation by skeletal muscle during dynamic isometric movements. IEEE Transactions on Biomedical Engineering 45:1010-1016

Brown IE, Loeb GE (2000) Measured and modeled properties of mammalian skeletal muscle: IV. Dynamics of activation and deactivation. Journal of Muscle Research and Cell Motility 21:33-47

Cegavske CF, Patterson MM, Thompson RF (1979) Neuronal unit activity in the abducens nucleus during classical conditioning of the nictitating membrane response in the rabbit. Journal of Comparative and Physiological Psychology 93:595-609

Choi JS, Moore JW (2003) Cerebellar neuronal activity expresses the complex topography of conditioned eyeblink responses. Behavioral Neuroscience 117:1211-1219

Cooper S, Eccles JC (1930) The isometric responses of mammalian muscles. Journal of Physiology 69:375-385

Curtin NA, Gardner-Medwin AR, Woledge RC (1998) Predictions of the time course and power output by dogfish white muscle fibres during brief tetani. Journal of Experimental Biology 201:103-114

Dean P (1996) Motor unit recruitment in a distributed model of extraocular muscle. Journal of Neurophysiology 76:727-742

Dean P, Porrill J, Warren PA (1999) Optimality of static force control by horizontal eye muscles: a test of the minimum norm rule. Journal of Neurophysiology 81:735-757

Delgado-García JM, Gruart A (2005) Firing activities of identified posterior interpositus nucleus neurons during associative learning in behaving cats. Brain Research Reviews 49:367-376

Ding J, Wexler JS, Binder-MacLeod SA (2002) A mathematical model that predicts the force-frequency relationship of human skeletal muscle. Muscle and Nerve 26:477-485

Disterhoft JF, Weiss C (1985) Motoneuronal control of eye retraction/nictitating membrane extension in rabbit. In: Neural Mechanisms of Conditioning (Alkon DL and Woody CD, Plenum, New York) 197-208

Dorgan SJ, O'Malley MJ (1998) A mathematical model for skeletal muscle activated by *N*-let pulse trains. IEEE Transactions on Rehabilitation Engineering 6:286-299

Eglitis I (1964) The glands. In: The Rabbit in Eye Research (Prince JH, Charles C. Thomas, Springfield, Il) 38-56

Evinger C, Manning KA, Sibony PA (1991) Eyelid movements. Mechanisms and normal data. Investigative Ophthalmology and Visual Science 32:387-400

Feldman AG (1981) The composition of central programs subserving horizontal eye movements in man. Biological Cybernetics 42:107-116

Fiala JC, Grossberg S, Bullock D (1996) Metabotropic glutamate receptor activation in cerebellar Purkinje cells as substrate for adaptive timing of the classically conditioned eye-blink response. Journal of Neuroscience 16:3760-3774

Freeman JH, Nicholson DA (2000) Developmental changes in eye-blink conditioning and neuronal activity in the cerebellar interpositus nucleus. Journal of Neuroscience 20:813-819

Garenne A, Chauvet GA (2004) A discrete approach for a model of temporal learning by the cerebellum: in silico classical conditioning of the eyeblink reflex. Journal of Integrative Neuroscience 3:301-318

Gluck MA, Allen MT, Myers CE, Thompson RF (2001) Cerebellar substrates for error correction in motor conditioning. Neurobiology of Learning and Memory 76:314-341

Goldberg SJ (1990) Mechanical properties of extraocular motor units. In: The Segmental Motor System (Binder MD and Mendell LM, Oxford University Press, New York) 222-238

Gruart A, Blázquez P, Delgado-García JM (1995) Kinematics of spontaneous, reflex, and conditioned eyelid movements in the alert cat. Journal of Neurophysiology 74:226-248

Gruart A, Schreurs BG, Del Toro ED, Delgado-García JM (2000) Kinetic and frequency-domain properties of reflex and conditioned eyelid responses in the rabbit. Journal of Neurophysiology 83:836-852

Hannaford B (1990) A nonlinear model of the phasic dynamics of muscle activation. IEEE Transactions on Biomedical Engineering 37:1067-1075

Hesslow G, Yeo CH (2002) The functional anatomy of skeletal conditioning. In: A Neuroscientist's Guide to Classical Conditioning (Moore JW, Springer, New York) 86-146

Hofstötter C, Mintz M, Verschure PFMJ (2002) The cerebellum in action: a simulation and robotics study. European Journal of Neuroscience 16:1361-1376

Hung G, Hsu F, Stark L (1977) Dynamics of the human eye blink. American Journal of Optometry and Physiological Optics 54:678-690

Huxley AF (1957) Muscle structure and theories of contraction. Progress in Biophysics and Biophysical Chemistry 7:257-318

Julian FJ (1969) Activation in a skeletal muscle contraction model with modification for insect fibrillar muscle. Biophysical Journal 9:547-570

Kernell D, Eerbeek O, Verhey BA (1983) Relation Between Isometric Force And Stimulus Rate In Cats Hindlimb Motor Units Of Different Twitch Contraction Time. Experimental Brain Research 50:220-227

Leal-Campanario R, Barradas-Bribiescas JA, Delgado-García JM, Gruart A (2004) Relative contributions of eyelid and eye-retraction motor systems to reflex and classically conditioned blink responses in the rabbit. Journal of Applied Physiology 96:1541-1554

Lennerstrand G (1974) Mechanical studies on the retractor bulbi muscle and its motor units in the cat. Journal of Physiology 236:43-55

Lepora NF, Mavritsaki E, Porrill J, Dean P, Yeo CH, Evinger LC (2005) Evidence for linearity in control of nictitating membrane responses by retractor bulbi motor units. In: 2005 Abstract Viewer/Itinerary Planner (Society for Neuroscience, Washington, DC) Prog. No. 869.863

Llinás R, Welsh JP (1993) On the cerebellum and motor learning. Current Opinion in Neurobiology 3:958-965

Mauk MD, Medina JF, Nores WL, Ohyama T (2000) Cerebellar function: Coordination, learning or timing? Current Biology 10:R522-R525

Mavritsaki E, Porrill J, Ivarsson M, Yeo CH, Dean P (2001) Recruitment of retractor bulbi motor units in a population model of the nictitating membrane response. Society for Neuroscience Abstracts 27:Prog. no. 405.404

McCormick DA, Thompson RF (1984) Neuronal responses of the rabbit cerebellum during acquisition and performance of a classically conditioned nictitating membrane-eyelid response. Journal of Neuroscience 4:2811-2822

Medina JF, Mauk MD (2000) Computer simulation of cerebellar information processing. Nature Neuroscience 3:1205-1211

Moore JW, Choi JS (1997) Conditioned response timing and integration in the cerebellum. Learning & Memory 4:116-129

Neidhard-Doll AT, Phillips CA, Repperger DW, Reynolds DB (2004) Biomimetic model of skeletal muscle isometric contraction: II. A phenomenological model of the skeletal muscle excitation-contraction coupling process. Computers in Biology and Medicine 34:323-344

Prince JH (1964) The rabbit in eye research. Charles C. Thomas, Springfield

Sanchez-Campusano R, Delgado-Garcia JM, Gruart A (2003) A phenomenological model for the neuromuscular control of reflex and learned eyelid responses. Society for Neuroscience Abstracts Program No:78.72

Shadmehr R, Arbib MA (1992) A Mathematical-Analysis Of The Force-Stiffness Characteristics Of Muscles In Control Of A Single Joint System. Biological Cybernetics 66:463-477

Shames DM, Baker AJ, Weiner MW, Camacho SA (1996) Ca2+-force relationship of frog skeletal muscle: a dynamics model for parameter estimation. American Journal of Physiology 271 (Cell Physiol. 40):C2061-C2071

Stein RB, Wong EY-M (1974) Analysis of models for the activation and contraction of muscle. Journal of Theoretical Biology 46:307-327

Thompson RF (1983) Neuronal substrates of simple associative learning: classical conditioning. Trends in Neuroscience 6:270-275

Trigo JA, Gruart A, Delgado-García JM (1999) Discharge profiles of abducens, accessory abducens, and orbicularis oculi motoneurons during reflex and conditioned blinks in alert cats. Journal of Neurophysiology 81:1666-1684

Trigo JA, Roa L, Gruart A, Delgado-García JM (2003) A kinetic study of blinking responses in cats. Journal of Physiology - London 549:195-205

Watanabe T, Futami R, Hoshimiya N, Handa Y (1999) An approach to a muscle model with a stimulus frequency-force relationship for FES applications. IEEE Transactions on Rehabilitation Engineering 7:12-18

Zahalak GI, Motabarzadeh I (1997) A re-examination of calcium activation in the Huxley cross-bridge model. Journal of Biomechanical Engineering 119:20-29

Zhou BH, Baratta R, Solomonow M (1987) Manipulation Of Muscle Force With Various Firing Rate And Recruitment Control Strategies. IEEE Transactions on Biomedical Engineering 34:128-139

Figure 1

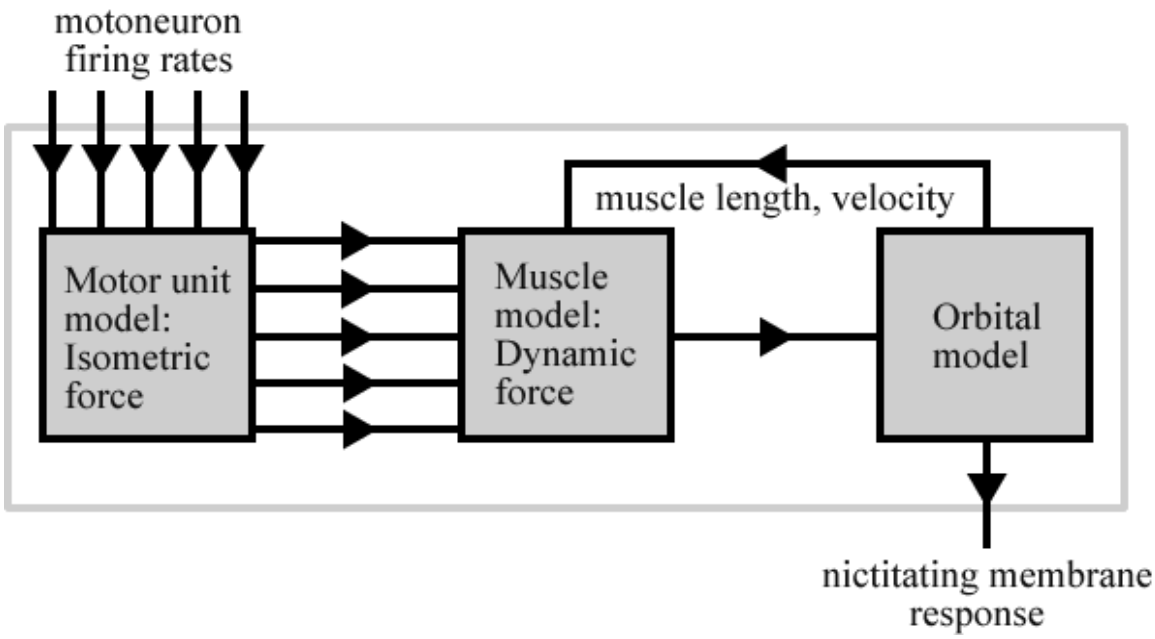

Overall structure of Bartha and Thompson's (1992a, 1992b) model of NMR production. The motoneurons whose firing rates form the input to the model are located in the accessory abducens nucleus, and the motor units that they control constitute the retractor bulbi muscle. The orbital model describes the mechanics of (i) the globe retraction produced by the action of the retractor bulbi muscle, and (ii) the extension of the nictitating membrane produced by globe retraction.

Figure 2

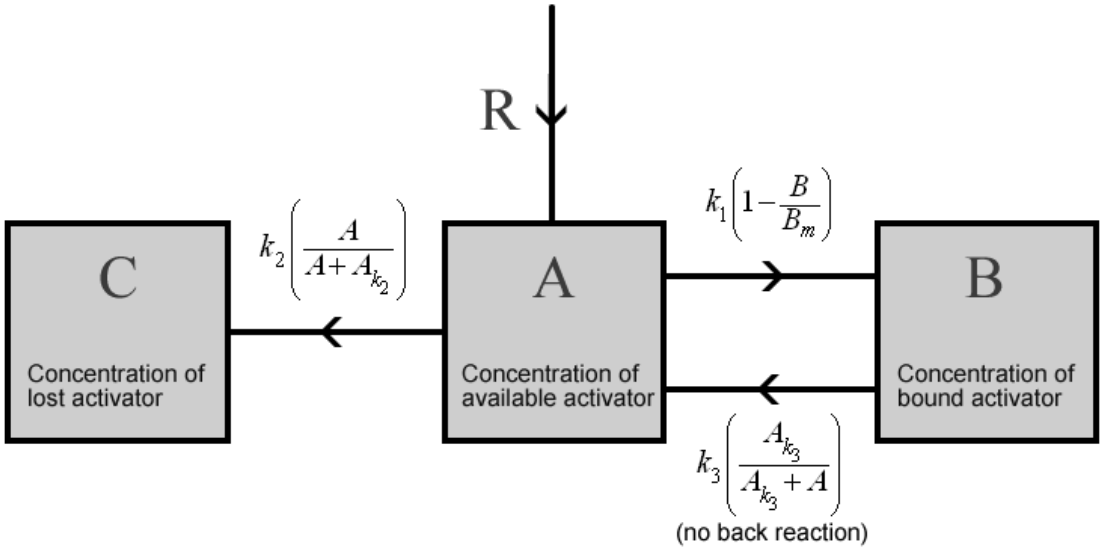

Activator kinetics in Bartha and Thompson's model. Neural impulses (represented by *R*) release free activator *A*, which is then either taken back up into the sarcoplasmic reticulum (*C*) or bound to the muscle (*B*) to produce muscle force. The formulae above the arrows denote the rates of the corresponding processes. The process whereby bound activator *B* returns to free activator affects *B* but not *A* (hence the label 'no back reaction').

Figure 3

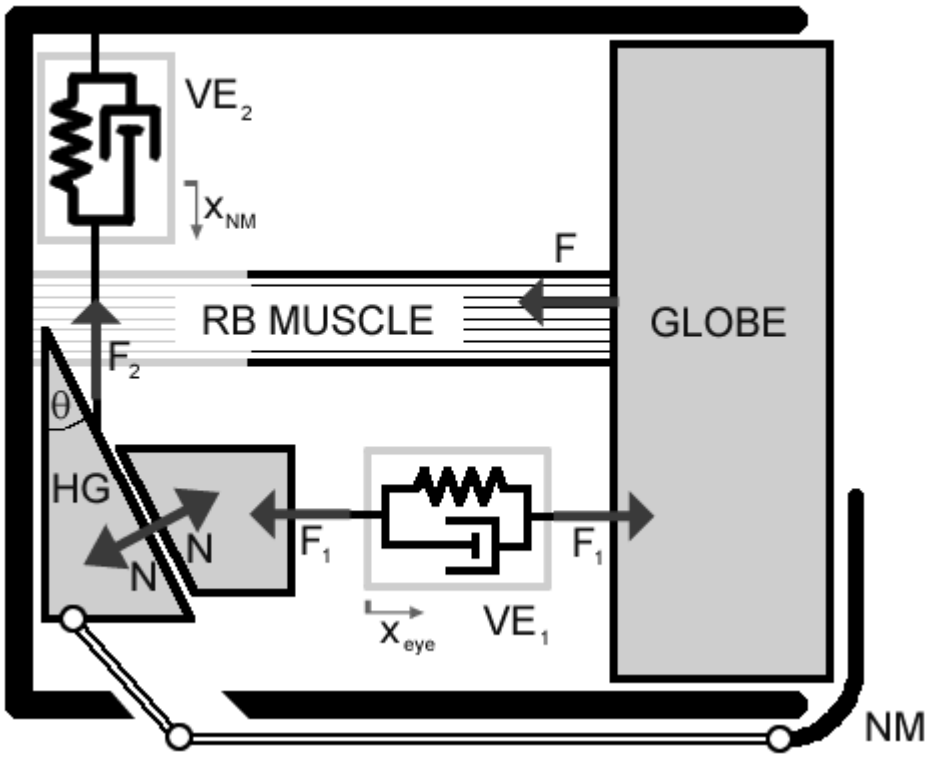

Orbital mechanics in Bartha and Thompson's model. Contraction of the RB muscle exerts a force *F=F(t)* at time *t* on the globe, causing it to retract. Globe retraction compresses orbital tissue (represented by a viscoelastic element VE_1) to produce a force $F_1=F_1(t)$ on Harder's gland HG, which is represented as a triangular block of tissue with a surface sloping at angle θ to the orbital wall. This geometry results in a force $F_2=F_2(t)$ parallel to the orbital wall, which acts via a second viscoelastic element VE_2 to move the gland. The nictitating membrane NM is attached rigidly to Harder's gland and moves with it. The force acting normal to the surface of Harder's gland is denoted by *N=N(t).*

Figure 4

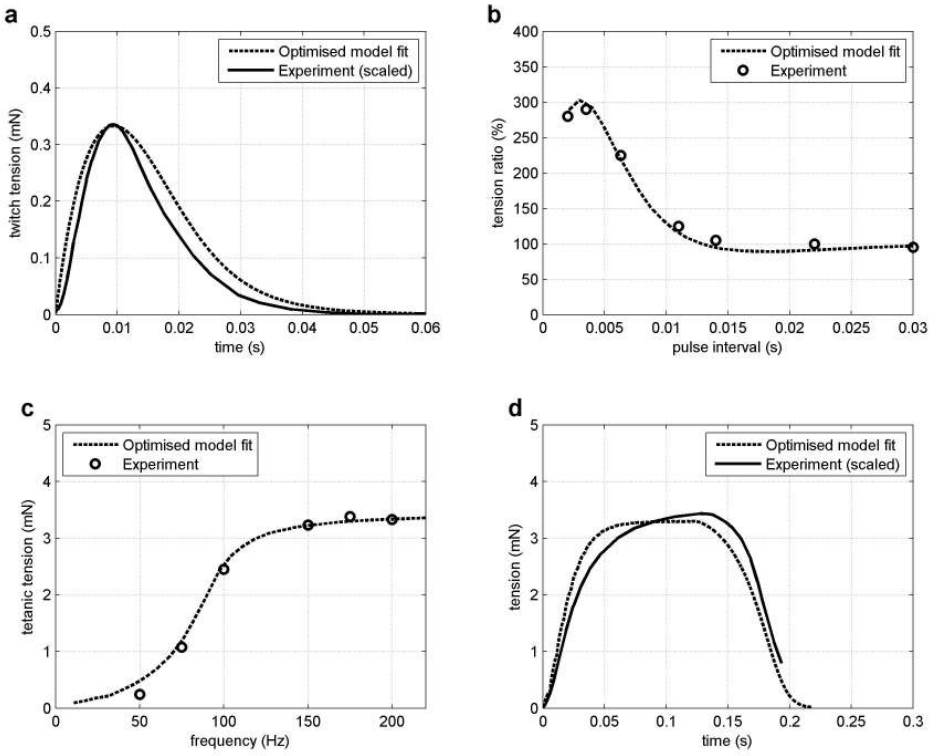

Simulated isometric-force response of model motor unit with optimised parameters, compared with experimental data from Lennerstrand (1974). Experimental motor unit strengths in panels a and d are taken from his Figs 2a and 4, and then scaled by values consistent with his Table 2. Tension ratios are taken from his Fig 3 and tetanic force from the motor unit values in his Fig 5.

a Time course of twitch response.

b Ratio of peak amplitudes of second and first twitches in response to two pulses, plotted against time interval between the pulses. The amplitude of the second twitch is measured with respect to the motor unit tension at its start.

c Steady state (averaged) tetanic isometric tension plotted against stimulus frequency.

d Development of isometric tension at a stimulus frequency of 175 Hz.

Figure 5

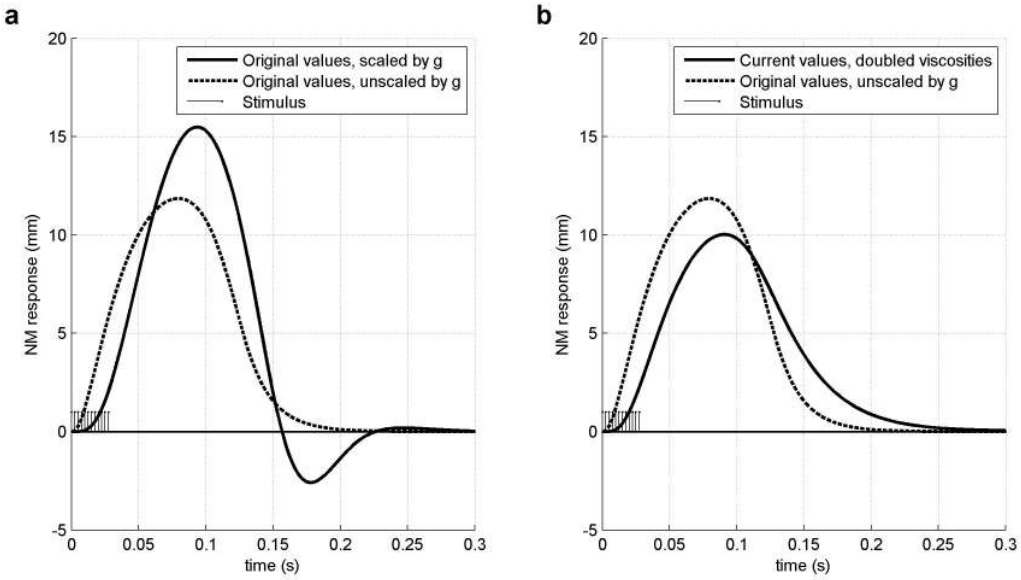

Simulated NMR to all 100 motoneurons firing at 400 Hz for 30 milliseconds.

a Response of the original model, as shown in Fig 1 of (Bartha and Thompson 1992a), with its inconsistent parameter values for orbital mass, viscosity and elasticity, compared with response when values are made consistent. In latter case the NMR overshoots noticeably on its return to baseline.

b Comparison of new model with original model. There is a small decrease in amplitude of around 20% together with an increase in latency from 10 to 20 msec.

Figure 6

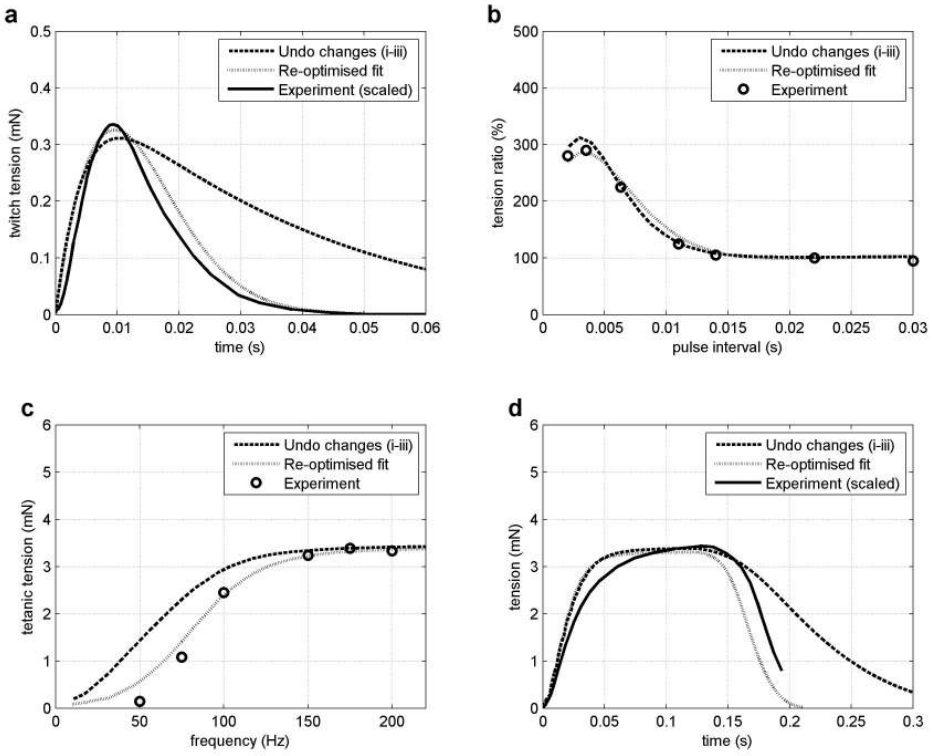

Effects of variations in activation equations on model performance, as indicated by the simulated isometric-force response of a model motor unit. 'Undo changes (i-iii)' indicates equations closer to those of Stein and Wong (see text); 'Re-optimised' indicates the Stein and Wong type equations with parameters specifically optimised to fit the shown experimental data (scaled as in Fig 4). Optimised parameter values: c = 0.96×9.81/1000, k_1 = 26, k_2 = 110, k_3 = 822, A_b = 0.34, B_m = 0.36, A_{k2} = 1.70, A_{k3} = 0.012, f_{max} = 0.99 and t_{peak} = 0.0043 (units as in Table 1). Panels as in Fig 4.

Figure 7

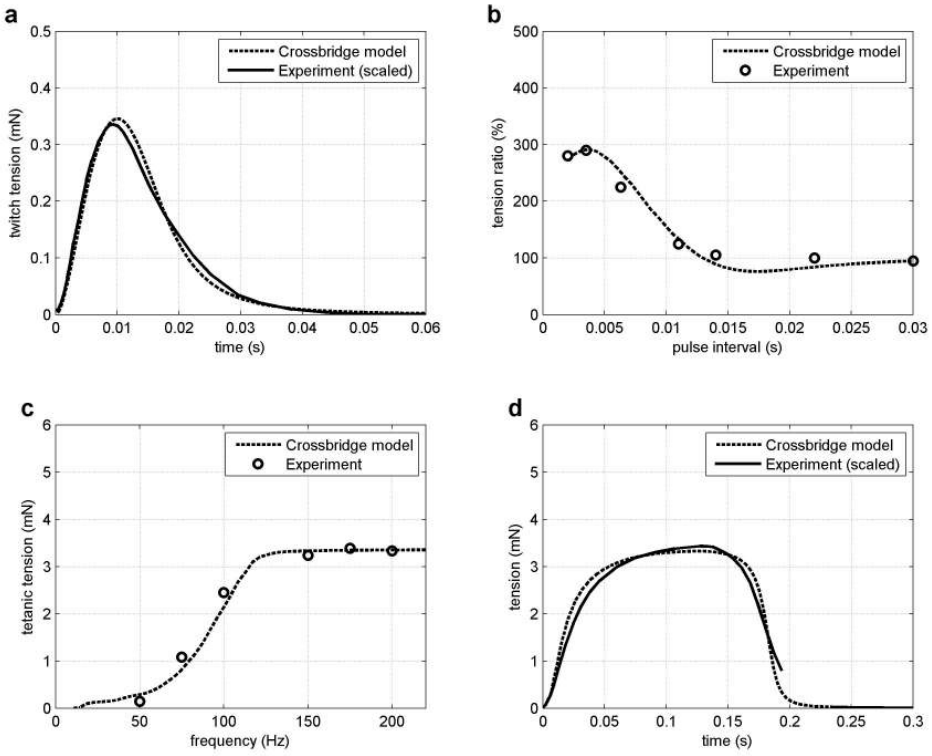

Performance of cross-bridge version of the model, compared with experimental data from Fig 4. Panels as in Figs 4 and 6. Optimised parameter values for cross-bridge model: k_1 = 220, k_2 = 50, k_3 = 1000, A_b = 0.053, B_m = 0.9, A_{k2} = 0.13, A_{k3} = 0.0014, f_{max} = 1.3 and t_{peak} = 0.005. Units as in Table 1. Parameter values varied between 25 and 400 percent of those in Table 1.

Figure 8

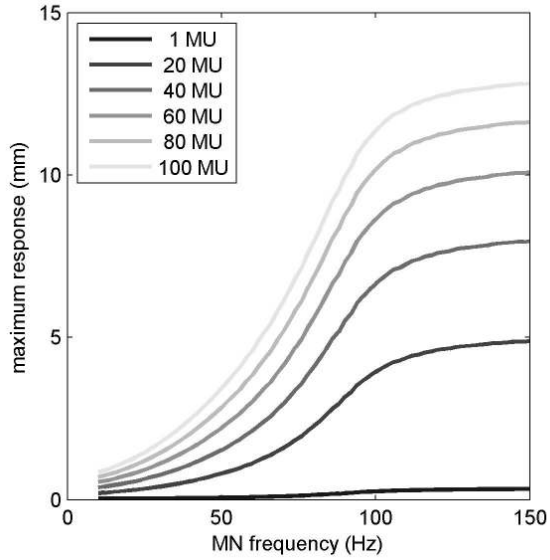

Response of model to rate-coding control strategy, as used by Bartha and Thompson (1992b). All MNs fire (i.e. no recruitment) at the same frequency. Graph shows the maximum NMR amplitude of model to MN firing as a function of MN firing frequency.

Figure 9

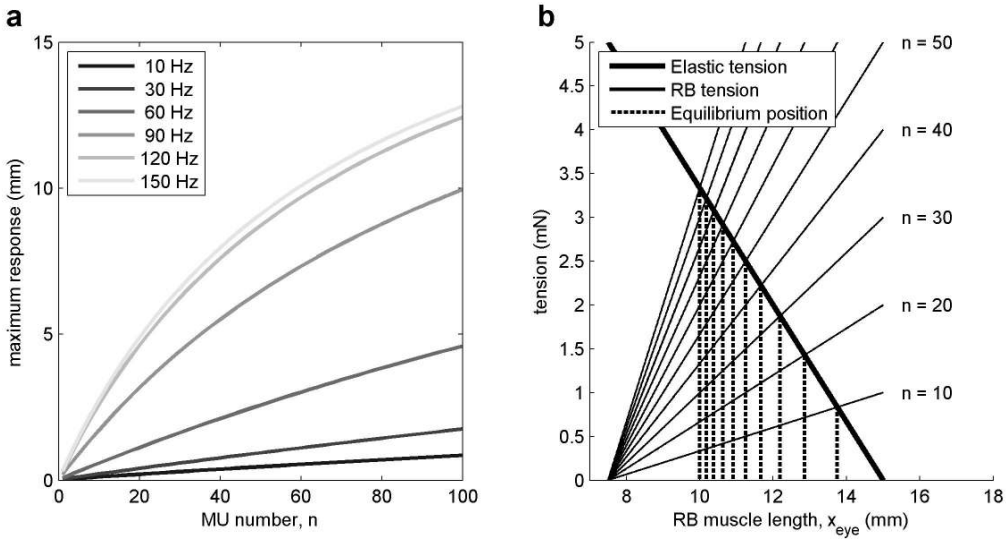

Response of model to simple recruitment control strategy. MNs either do not fire at all, or fire at a given constant frequency.

a Amplitude of NMR as a function of number of units recruited, at different frequencies of firing for the recruited units.

b Effects of recruitment on muscle length-tension curves. The intersections of these curves (thin black lines) with the corresponding length tension curve for orbital tissue (thick black line), determine the equilibrium points of the system. The dashed lines indicate the muscle lengths at those equilibrium points. As the number of recruited units scales linearly, the equilibrium position varies non-linearly.

Figure 10

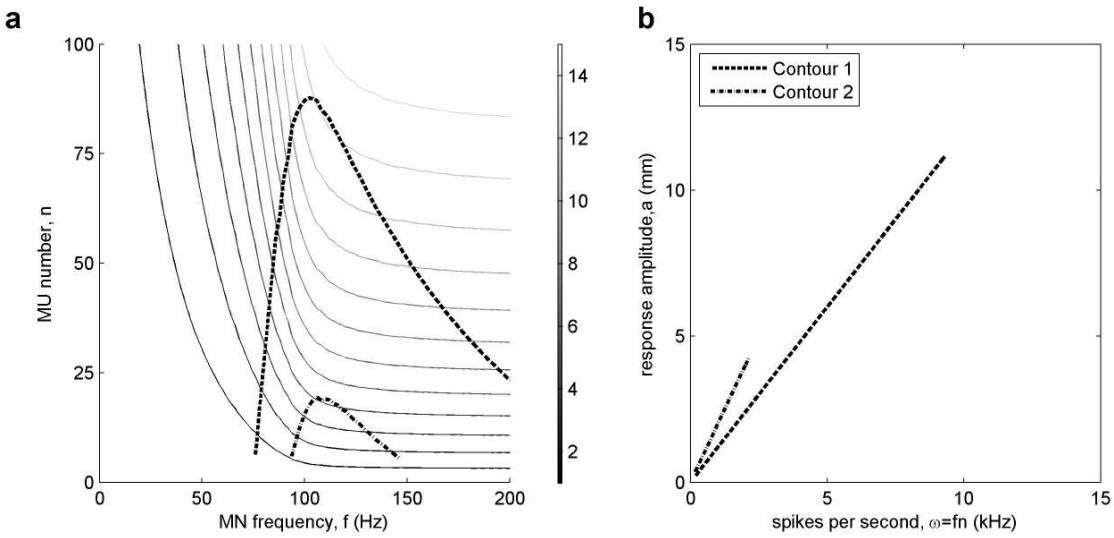

Response of model when recruitment is combined with rate coding, i.e. both unit number and frequency are allowed to vary.

a Grayscale curves show the contours of maximum response amplitude *a* for *n* motor units firing at frequency *f*. The dotted curves track where the maximum amplitude *a(f,n)* is proportional to the total spike number $\omega = fn$.

b The straight lines display the response amplitudes *a* generated by the curves of linear response to total spike frequency ω displayed in panel **a**.

Figure 11

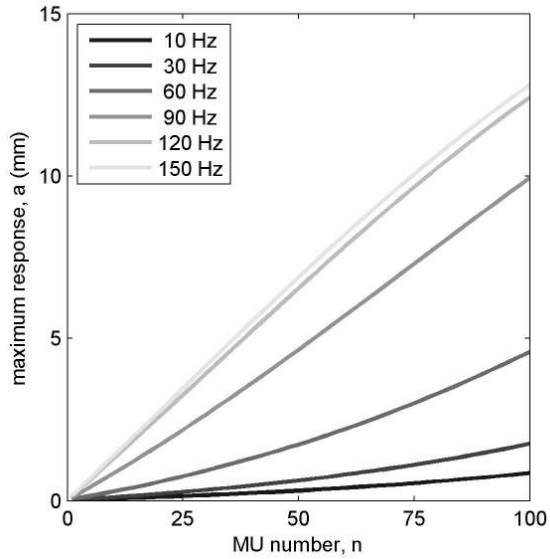

Response of model to stimuli of constant frequency *f* when the n_{max}=100 motor unit strengths vary according to an exponential distribution $\exp(b\, i/n_{max})$ for the *i* th MU. Note the approximately linear relationship, particularly for frequencies >60 Hz.

Table 1

Parameter	Value	Parameter	Value
c	$0.4\times9.81\times10^{-3}$ N/μmol	L_1	0.12
k_1	100 μmol/s	L_2	0.8×10^{3} m^{-1}
k_2	50 μmol/s	a / F_0	0.3
k_3	250 μmol/s	$v_{\max}$	-0.44 m/s
B_m	0.9 μmol		
A_{k_2}	1 μmol	M_{eye}	3×10^{-3} kg
A_{k_3}	0.05 μmol	M_H	1.5×10^{-3} kg
A_b	0.22 μmol	θ	0.31 rad
$f_{\max}$	1.35	k_g	116 N/m
t_{peak}	3.5×10^{-3} s	k_H	2.9 N/m
A_{m}	2.5 μmol	ν_g	$70.3\times9.81\times10^{-3}$ Ns/m
		ν_H	$16.3\times9.81\times10^{-3}$ Ns/m
n	100	x_{k_g}	15.1×10^{-3} m
k_p	3.5 N/m	x_{k_H}	-1.53×10^{-3} m
x_{rest}	11×10^{-3} m		

Table 1: Parameter values used in the model in SI units.

Table 2

Parameter	Values (SI units)				
	Figs 1 & 2	Figs 3 & 4	Fig 5	Table 1	Optimised
c (N/μmol)	$0.475\times9.81\times10^{-3}$	$0.37\times9.81\times10^{-3}$	$0.44\times9.81\times10^{-3}$	$0.475\times9.81\times10^{-3}$	$0.40\times9.81\times10^{-3}$
k_1 (μmol/s)	120	101	120	101	100
k_2 (μmol/s)	50	41.5	50	41.5	50
k_3 (μmol/s)	275	230	275	230	250
A_b (μmol)	0.2	0.18	0.15	0.18	0.22

Table 2: Variants of parameter values used in original model, compared with optimised values. Figs 1-5 refer to the corresponding figures in Bartha and Thompson (1992b). Table 1 refers to Table 1 of Bartha and Thompson (1992a). The optimised values were derived as explained in the text. Additional optimised parameter values that differed from those in Table 1 were: B_m=1.0 μmol (original) to B_m=0.9 μmol (optimised); f_{max}=1.3 (original) to f_{max}=1.35 (optimised); and t_{peak}=4 ms (original) to t_{peak}=3.5 ms (optimised). Changes to parameter values were typically less than 20%.

Table 3

Parameter	Value	Parameter	Value
s/h	1/100000	a/F_0	0.3
g_1/f_1+g_1	0.21	F_0	0.35 N
g_2/f_1+g_1	3.25	v_{max}	-0.44 m/s
f_1+g_1	1320		
e_0	1.3×10^{-4} J		
k_0	0.87 N/m		

Table 3: Parameter values for the cross-bridge model. Units as in Table 1.